Helsinki University of Technology
Inorganic Chemistry Publication Series
Espoo 2002 No. 3

CONTROL OF COPPER AND IRON OXIDATION STATES IN SOME TRIPLE- AND DOUBLE-PEROVSKITE OXIDES

Kaisa Lehmus

Helsinki University of Technology
Inorganic Chemistry Publication Series
Espoo 2002 No. 3

CONTROL OF COPPER AND IRON OXIDATION STATES IN SOME TRIPLE- AND DOUBLE-PEROVSKITE OXIDES

Kaisa Lehmus (*née* Peitola)

Dissertation for the degree of Doctor of Science in Technology to be presented with due permission of the Department of Chemical Technology for public examination and debate in Auditorium KE 2 at Helsinki University of Technology (Espoo, Finland) on the 26th of April, 2002, at 12 noon.

Helsinki University of Technology
Department of Chemical Technology
Laboratory of Inorganic and Analytical Chemistry

Teknillinen korkeakoulu
Kemian tekniikan osasto
Epäorgaanisen ja analyyttisen kemian laboratorio

Distribution:
Helsinki University of Technology
Laboratory of Inorganic and Analytical Chemistry
P.O. Box 6100
FIN-02150 HUT, FINLAND

ISBN 951-22-5920-6
ISSN 1458-5154

Picaset Oy
Helsinki 2002

ABSTRACT

This thesis consists of eight publications and a summary of the obtained experimental results, reviewed together with the most essential literature related to the topic. The work deals with ways of tuning and analyzing the transition metal oxidation states in the superconductive $Cu(Ba,Sr)_2(Yb,Ca)Cu_2O_{6+z}$ triple perovskite and the $BaRE(Fe,Cu)O_{5+\delta}$ double perovskite, which has aroused interest as a structure potentially exhibiting both superconductivity and magnetoresistivity. These triple- and double-perovskite oxides are compared with regard to their charge distribution at different cation and oxygen stoichiometries. Complementary methods of analysis, including both chemical and physical techniques, are utilized for the determination of the charge distribution in these layered oxide structures with several transition metal ions. Multivariate data analysis is introduced as a novel way for examining the structure-property correlations of complex oxide structures based on the crystallographic data obtained by neutron diffraction.

The Ca(II)-for-*RE*(III) substituted and oxygen-doped $Cu(Ba_{0.8}Sr_{0.2})_2(Yb_{1-x}Ca_x)Cu_2O_{6+z}$ triple perovskites ($0 \leq x \leq 0.35$ with $z \approx 0$ and $0 < z < 1$ with $x = 0$) are described for their fine structures and the charge distribution over the unit cell is determined by two different methods. Bond-valence-sum (BVS) calculations based on structural data obtained by neutron diffraction are shown to be a convenient means to study small gradual changes in the fine structure and the charge distribution. O *K*-edge and Cu $L_{2,3}$-edge XANES results independently showed same trends in the charge distribution as did the BVS calculations, *i.e.* stronger oxidation of the superconductive part of the structure by Ca(II)-for-*RE*(III) substitution than by oxygen doping.

The oxygen stoichiometry of the $BaRE(Fe_{0.5}Cu_{0.5})_2O_{5+\delta}$ double perovskite is shown to depend on the size of the RE^{3+} ion and on the oxygen partial pressure during the final heat treatment of the synthesis. Under ambient pressure, the excess oxygen atom δ can be inserted only in the structures with largest *RE*s (Nd and Pr) whereas high-pressure treatment ($p = 5$ GPa) was found to stabilize δ also in the structures with smaller *RE*s. The charge distribution between copper and iron is studied by means of coulometric titration and ^{57}Fe Mössbauer spectroscopy. In the normal-pressure oxygenated samples only Fe(III) is oxidized to higher oxidation states, but high-pressure heat treatment enables oxidation of Cu(II) to Cu(III) as well. The excess oxygen can be removed from all compounds by deoxidative post-annealing performed in a controlled way in a thermobalance.

PREFACE

The experimental work of this thesis was carried out in the Laboratory of Inorganic and Analytical Chemistry at the Helsinki University of Technology (HUT) between August 1998 and May 2001. The work is part of a collaboration project between HUT and the Tokyo Institute of Technology (TIT).

I am deeply grateful to my advisor Prof. Maarit Karppinen, now at TIT, for providing me the opportunity to work in a research project of high international level. It has been a pleasure to work under her inspiring and expert supervision. I also wish to express my warm gratitude to Prof. Lauri Niinistö for his continuous support throughout my studies.

I am greatly indebted to my co-authors for their expert input with different characterization techniques. I owe special thanks to Dr. Johan Lindén from Åbo Academi University for the Mössbauer spectroscopy measurements, and for sharing some nice moments during my trips to Japan. I want to express my sincere gratitude also to Prof. Hisao Yamauchi, Dr. Takayuki Nakane and Mr. Motoki Kochi at the Materials and Structures Laboratory for fruitful collaboration and for the interesting stay at TIT in summer 1998 and autumn 1999. Prof. Roland Tellgren and Dr. Håkan Rundlöf from Uppsala University are thanked for the neutron diffraction measurements and for their advice with structure refinements. I am further grateful to the group of Prof. Liu in Taiwan for collaboration with the XANES measurements. I also want to express many thanks to the other students of the perovskite-oxide group, Lic. Phil. Miia Kotiranta, Mr. Mikko Matvejeff and Ms. Kirsi Salomäki, for all their help and the inspiring discussions. I am greatly thankful to the whole personnel in the Laboratory of Inorganic and Analytical Chemistry for creating a nice working atmosphere.

My present employer, Vaisala Oyj, is thanked for providing the opportunity to finalize this work. Mr. Philip Canty's kind help with the language of the thesis is greatly appreciated. Finally, I warmly thank my family, particularly my husband Matti, for support and patience during these busy months.

Jenny and Antti Wihuri Foundation, the Finnish Foundation of Technology, Emil Aaltonen Foundation and the Academy of Finland are all gratefully acknowledged for financial support.

Helsinki, March 2002

Kaisa Lehmus

LIST OF PUBLICATIONS

In addition to the present review, the dissertation includes the following publications, which are referred to in the text by the corresponding Roman numerals:

I Karppinen, M., Yamauchi, H., Fujinami, K., Nakane, T., Peitola, K., Rundlöf, H., and Tellgren, R., Ca-Substitution and O-Doping Effects in Superconducting $Cu(Ba_{0.8}Sr_{0.2})_2(Yb_{1-x}Ca_x)Cu_2O_{6+z}$ Obtained from Neutron Diffraction Refinements, *Phys. Rev. B* **60** (1999) 4378-4385.

II Karppinen, M., Yamauchi, H., Nakane, T., Fujinami, K., Lehmus, K., Nachimuthu, P., Liu, R.-S., and Chen, J.M., XANES Study on the Generation and Distribution of Holes *via* Ca-substitution and O-doping in $Cu(Ba_{0.8}Sr_{0.2})_2(Yb_{1-x}Ca_x)Cu_2O_{6+z}$, *J. Solid State Chem.*, in press.

III Lehmus, K. and Karppinen, M., Application of Multivariate Data Analysis Techniques in Modeling Structure-Property Relationships of Some Superconductive Cuprates, *J. Solid State Chem.* **162** (2001) 1-9.

IV Peitola, K., Kochi, M., Karppinen, M., Yamauchi, H., Niinistö, L., and Lindén, J., Oxygen Stoichiometry in Ba*RE*$(Cu_{0.5}Fe_{0.5})_2O_{5+\delta}$ Compounds with Perovskite or Double Perovskite Structure, *J. Low Temp. Phys.* **117** (1999) 861-865.

V Lehmus, K., Kochi, M., Karppinen, M., Yamauchi, H., and Niinistö, L., Variation of Oxygen Stoichiometry in Ba*RE*$(Cu_{0.5}Fe_{0.5})_2O_{5+\delta}$ Double Perovskites upon Heat Treatments under Ambient and High Pressure, *Int. J. Inorg. Mater.* **2** (2000) 203-208.

VI Lehmus, K., Karppinen, M., Matvejeff, M., Lindén, J., Pietari, T., and Yamauchi, H., Oxygen Stoichiometry in the $(Ba_{0.5}La_{0.5})(Fe_{1-x}Cu_x)O_{3-w}$ (x = 0-1) Perovskite System, *Int. J. Inorg. Mater.* **3** (2001) 803-808.

VII Lindén, J., Kochi, M., Lehmus, K., Pietari, T., Karppinen, M., and Yamauchi, H., Interplay between Cu and Fe Valences in Ba*R*$(Cu_{0.5}Fe_{0.5})_2O_{5+\delta}$ Double Perovskites with *R* = Lu, Yb, Y, Eu, Sm, Nd, and Pr, *J. Solid State Chem.*, in press.

VIII Kochi, M., Lindén, J., Taniyama, T., Lehmus, K., Karppinen, M., and Yamauchi, H., Magnetic Properties, Oxygen Content and Metal Valences in Ba*RE*$(Cu_{0.5}Fe_{0.5})_2O_{5+\delta}$ with *RE* = Lu, Yb, Y, Eu, Sm, Nd and Pr, *Physica C* **338** (2000) 132-136.

THE AUTHOR'S CONTRIBUTION TO THE APPENDED PUBLICATIONS

Publications **I** and **II**	The author has carried out neutron diffraction refinements and the calculations based on the refinements and taken part in preparation of the manuscript.
Publication **III**	The author has defined the research plan together with M. Karppinen, carried out the experiments, interpreted results and written the manuscript.
Publications **IV-VI**	The author has defined the research plan together with M. Karppinen, carried out the experiments with the normal-pressure synthesized samples, interpreted the results, excluding Mössbauer spectroscopy, and written the manuscripts.
Publications **VII** and **VIII**	The author has synthesized the normal-pressure samples, analyzed their oxygen contents and provided input for the co-authors during preparation of the manuscripts.

LIST OF SYMBOLS AND ABBREVIATIONS

Abbreviations in chemical formulae

A	Large metal, *e.g.* Ba, Sr, La, in the *A* site of the perovskite structure
B	*d*-block transition metal, *e.g.* Mn, Fe, Co, Cu, in the *B* site of perovskite structure
Q	Intermediate-size metal, *e.g. RE*, Ca
M_m	Metal (*M*), *e.g.* Cu, Pb, Bi, Hg, and its stoichiometry (*m*) in the charge reservoir block of superconductive copper oxides
n	Number of superconducting CuO_2 planes
RE	Rare earth element (Sc, Y and the lanthanides La - Lu)
z, δ	Amount of excess oxygen
w	Amount of oxygen deficiency

Other abbreviations and symbols

BVS	Bond Valence Sum
CN	Coordination Number
MR	Magnetoresistivity
NPD	Neutron Powder Diffraction
PC	Principal Component
PCA	Principal Component Analysis
PLS	Projections to Latent Structures by means of partial least squares
$p(CuO_2)$	Hole concentration of an individual CuO_2 plane
redox	Reduction-oxidation
R_{ij}	Bond length *i-j*
R_{ij}^0	BVS scaling parameter for the *i-j* bond
s_{ij}	Bond valence of the *i-j* bond
T_c	Superconductivity transition temperature
V_i	Oxidation state of species *i*
XANES	X-ray Absorption Near-Edge Structure

CONTENTS

1. INTRODUCTION

Perovskite-type oxides have attracted considerable attention as they display a rich diversity of chemical compositions and fascinating electrical, magnetic, optical and catalytic properties. The versatility of properties is demonstrated for example by the electrical conductivity which varies in a wide range from highly insulating to semiconductive, metallic and even superconductive properties depending on the chemical composition of the perovskite structure. Additionally, some perovskites exhibit ionic conductivity or mixed electronic and ionic conductivity. The discovery of high-temperature superconductivity in perovskite-related copper oxides in 1986 soon lead to enormous research efforts in different fields of materials science in order to develop and prepare even better superconductive materials. More recently, magnetoresistivity (MR) was observed in some perovskites and part of the attention in the perovskite research was turned to this interesting phenomenon. Superconductivity and magnetoresisitivity are both material properties related to the dependence of electrical resistivity on temperature and external magnetic field strength. Besides structural similarity, occurrence of a transition metal in a mixed oxidation state is common to superconductive and magnetoresistive perovskites. Understanding the role of the mixed oxidation state and the ways of controlling it in these structures is considered vitally important for tailoring new materials with desired properties. The present thesis deals with the control and determination of the transition metal mixed oxidation state in perovskite-related oxides.

This work is part of a research collaboration project between Helsinki University of Technology and Tokyo Institute of Technology. The main aim of the research is to understand the structure-property relations of perovskite-type transition metal oxides and, based on this understanding, to develop new superconductive and magnetoresistive materials. Generally, the knowledge of perovskite chemistry obtained in the research of copper oxide superconductors is now being utilized in the research of other perovskite oxides for a variety of applications.

1.1 *A*-site ordered triple- and double-perovskite structures

The variety of different properties observed for perovskite-related oxides is explained by the flexibility of the perovskite structure ABO_{3-w} which allows for distortions, oxygen non-stoichiometry and cation substitutions. Ordering of cations is probable when the *A* or *B* site in ABO_{3-w} is co-occupied by two or several cations with different ionic radii, oxidation states and/or coordination properties.[1] *A*-site ordering is observed *e.g.* with a divalent alkaline earth metal and a trivalent rare earth element (*RE*) and it leads to the formation of a double-perovskite or a triple-perovskite structure depending on the ratio of cations. Ordering of the *A*-site cations usually results in oxygen vacancies around the smaller of the cations, *i.e.* RE^{3+}, which generally prefers coordination numbers (CN) lower than 12. As the oxygen vacancies are produced, the coordination polyhedron of the transition metal cation in the *B* site changes from an octahedron (CN = 6) to a square pyramid (CN = 5).

Of the *A*-site ordered perovskites, high-temperature superconductive $CuBa_2RECu_2O_{6+z}$ triple perovskite is the best-known example.[2] In its layered CuO_z-BaO-CuO_2-*RE*-CuO_2-BaO structure, the *RE* layer is oxygen free and copper has two different environments in the square pyramidal CuO_5 and square planar CuO_z units. The oxygen content in CuO_z can be tuned continuously in the range of $0 \leq z \leq 1$ with a tetragonal to orthorhombic transition at $z \approx 0.45$. Superconductivity appears at $z \approx 0.45$ and the critical temperature (T_c) increases monotonically with the oxygen content.[3] The unit cell of $CuBa_2RECu_2O_{6+z}$ (*RE* = Y) and the notation system used for the atoms are presented in Figure 1a. The oxygen-deficient triple-perovskite structure is formed with several cation stoichiometries both at the *A* and the *B* site, and different compositions have been frequently studied in order to reach a better understanding of the mechanism of high-T_c superconductivity. The triple-perovskite structures of iron, *e.g.* $FeBa_2YFe_2O_8$[4], and cobalt, *e.g.* $CoK_{0.5}Ba_{1.5}YCo_2O_8$[5], are otherwise similar to $CuBa_2YCu_2O_{6+z}$ but instead of the square planar coordination observed for copper in the CuO_z unit, iron and cobalt have an octahedral coordination. Furthermore, in these structures the probability of an excess oxygen atom in the *RE* layer is increased.

The $CuBa_2RECu_2O_{6+z}$ triple perovskite belongs to the group of superconductive copper oxide phases which have all layered perovskite-related structures. These structures are built up of alternating $M_mO_{m\pm z}$ blocks (oxygen-deficient perovskite or rock-salt type structure; *M* = *e.g.* Cu, Bi, Pb, Tl, Hg; *m* = 0-3), *A*O layers (rock-salt structure; *A* = Sr, Ba, La) and $Q_{n-1}Cu_nO_{2n}$

blocks (oxygen-deficient perovskite structure; Q = Ca, *RE*; n = 1-7). Based on the stacking of these blocks the structures can be classified as members of different $M_mA_2Q_{n-1}Cu_nO_{2+2n\pm z}$ or *M*-*m*2(*n*-1)*n* homologous series.[6,7] Common to all these structures are the CuO_2 planes which are needed for the electric transport.

$BaY(Fe_{0.5}Cu_{0.5})_2O_{5+\delta}$ with alternating BaO and YO_δ layers was the first well-characterized copper oxide with an *A*-site ordered double-perovskite structure (Figure 1b).[8] Later the $BaRE(Fe_{0.5}Cu_{0.5})_2O_{5+\delta}$ double perovskite was shown to be formed with several other rare earths and oxygen stoichiometries.[9] The structure is also known with the *B* site containing other transition metals than Fe and Cu as in $BaRE(Co_{1-x}Cu_x)_2O_{5+\delta}$ (*RE* = Y; $0 < x \leq 0{,}5$)[10], $BaRE(Fe_{0.5}Co_{0.5})_2O_{5+\delta}$ (*RE* = Y, La)[11,12], $BaREFe_2O_{5+\delta}$ (*RE* = Sm, Nd)[13,14], $BaRECo_2O_{5+\delta}$ (*RE* = Y, Pr, Nd, Sm, Eu, Gd, Tb, Dy, Ho)[15-17] and $BaREMn_2O_{5+\delta}$ (*RE* = Y, La)[18-21]. In the double-perovskite structure the oxygen content can be varied in the REO_δ layer if the *B* metal can be oxidized and if the coordination numbers higher than 8 are prefered by the *RE*, meaning the larger *RE* ions.[22] Even though the double- and triple-perovskite structures are otherwise similar, the lack of the $M_mO_{m\pm z}$ block in the double-perovskite structure causes significant differences in the charge balance and the material properties. Unlike the $CuBa_2RECu_2O_{6+z}$ triple perovskite, the $BaREB_2O_{5+\delta}$ double perovskite has not shown superconductivity since its stabilization with solely copper in the *B* site has not been successful.[23,24]

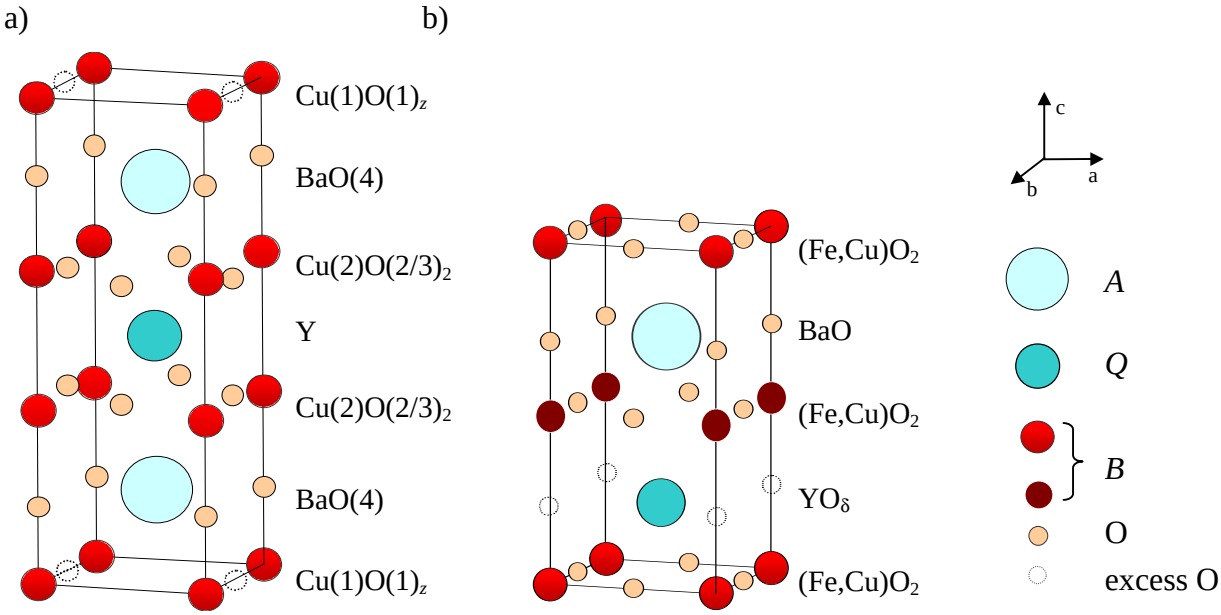

Figure 1. a) Triple-perovskite structure, *e.g.* $CuBa_2YCu_2O_{6+z}$, and b) double-perovskite structure, *e.g.* $BaY(Fe_{0.5}Cu_{0.5})_2O_{5+\delta}$.

1.2 Role of the transition metal oxidation state and coordination number in perovskites

Structural distortions and non-stoichiometry are common in perovskite-type structures. Due to the versatile coordination and reduction-oxidation (redox) chemistry of transition metals in the *B* site, the perovskite structure allows cation or oxygen non-stoichiometry within certain limits. The *B*-site cation has a prominent role in determining the electrical, magnetic and catalytic[25,26] properties of the perovskite-type materials. The appearance of superconductivity in the copper oxide structures is related to a partial oxidation of copper to the trivalent state in the CuO_2 planes. When a CuO_2 plane is oxidized, the T_c increases in the under-doped region to the level of optimal doping above which the material is over-doped and the T_c starts to drop. At optimal doping the oxidation state of copper in the CuO_2 planes has empirically been determined to be ~ +2.15.[6] Distribution of the total oxidation over the unit cell is also essential and, in addition to the T_c, it also influences other superconductivity properties such as the critical current characteristics.[6]

The important role of the copper mixed Cu(II)/(III) oxidation state for superconductivity in copper oxides is well established but magnetoresistivity in some manganese (Mn(III/IV))[27,28], cobalt (Co(II/III/IV))[15,28] and iron (Fe(II/III/IV/V))[29,30] oxides is also related to the mixed oxidation state of the transition metal. Magnetoresistivity effect has been observed in both simple and ordered perovskite structures. In the *A*-site ordered double-perovskite structure, the MR effect was observed for the first time for cobalt oxides[16] whose magnetic and electrical properties are controlled by the oxygen content and ordering of oxygen atoms, both of which depend on the size of the *RE* constituent.[16,31,32] Also the iron-based $BaSmFe_2O_{5+\delta}$ double perovskite[14] and the $La_{1/3}Sr_{2/3}FeO_{3-w}$ perovskite[30] have been found to possess magnetoresistive properties. In $BaSmFe_2O_{5+\delta}$, the MR effect is related to the mixed-valence state of iron $Fe^{2.5+}$ which is demonstrated by the fact that the MR possesses a peak at the temperature where $Fe^{2.5+}$ separates to Fe(II) and Fe(III).[29] Increasing the oxygen content from $\delta \approx 0$ decreases both the strength of the MR effect and the temperature at which it is observed. Similarly in $La_{1/3}Sr_{2/3}FeO_{3-w}$, the MR peak appears at the temperature where tetravalent iron disproportionates to tri- and pentavalent iron. This disproportionation leads to charge ordering and to a magnetic transition from paramagnetic to antiferromagnetic state.[30]

Varying the oxygen non-stoichiometry in a perovskite-type structure is a straightforward way to control the transition metal oxidation state but substituting a cation by a lower or a higher

valent cation also forces the transition metal to change the oxidation state. Tuning the oxygen stoichiometry in the *A*-site ordered triple- and double-perovskite structures has a different effect on the charge distribution due to the differing location of the excess oxygen in these structures. In the Ba*REB*$_2$O$_{5+\delta}$ double perovskite, the possible excess oxygen atom is located in the *RE* layer between two *B*O$_2$ planes thus destroying the square pyramidal coordination of the transition metal. From the superconductivity point of view an excess oxygen atom in the *RE* layer would most probably be detrimental. Therefore, oxidation of divalent copper and appearance of superconductivity in the double-perovskite structure is supposed to be achieved only by suitable cation substitutions at $\delta = 0$.[6] On the other hand, superconductive properties of the CuBa$_2$*RE*Cu$_2$O$_{6+z}$ triple perovskite can be controlled by tuning the valence of copper in the CuO$_2$ plane either by cation substitutions or by varying the oxygen content in the CuO$_z$ layer.

1.3 Scope of the present thesis

The aim of the present work was to establish the ways of tuning and analyzing the charge distribution in Cu*A*$_2$*RE*Cu$_2$O$_{6+z}$ triple-perovskite and Ba*REB*$_2$O$_{5+\delta}$ double-perovskite structures. The effectiveness of cation substitution and oxygen doping in creating positive holes and increasing the T_c were studied in the Cu(Ba$_{0.8}$Sr$_{0.2}$)$_2$(Yb$_{1-x}$Ca$_x$)Cu$_2$O$_{6+z}$ system.[I,II] In order to independently study the different ways of creating holes, two sample series, *i.e.* a series of Ca-for-Yb substituted ($0 \le x \le 0.35$, $z \approx 0$) samples and a series of samples with different oxygen contents ($0 < z < 1$, $x = 0$), were prepared and characterized for their fine structures and superconductivity properties.[I] Bond-valence-sum calculations based on powder neutron diffraction data and O *K*-edge and Cu $L_{2,3}$-edge XANES (X-ray Absorption Near Edge Structure) spectroscopy measurements were utilized for studying the charge distribution in the structure.[I,II] Applicability of multivariate data analysis methods for studying structure-property relations of ionic compounds was explored by analyzing the T_c values and the structural data of Cu*A*$_2$*Q*Cu$_2$O$_{6+z}$ triple perovskites with varying combinations of *A*, *Q* and *z* as multivariate data.[III]

Unlike in Cu*A*$_2$*RE*Cu$_2$O$_{6+z}$ triple perovskites, oxygen stoichiometry in Ba*REB*$_2$O$_{5+\delta}$ double perovskites can be varied under normal pressure in the structures with certain cation compositions only. In order to study ways of tuning the transition metal oxidation states in the

Ba*RE*$(Fe_{0.5}Cu_{0.5})_2O_{5+\delta}$ double perovskite, samples with different *RE*s were exposed to heat treatments under normal- and ultra high-pressure conditions.[IV-VI] The resulting charge distribution between copper and iron was established by combining the results of wet-chemical methods, thermogravimetry and ^{57}Fe Mössbauer spectroscopy.[IV,V,VII] The magnetic properties of the Ba*RE*$(Fe_{0.5}Cu_{0.5})_2O_{5+\delta}$ double-perovskite samples were also considered.[VIII]

2. DETERMINATION OF Cu AND Fe OXIDATION STATES

Since oxidation state and coordination number of the transition metal constituent have a crucial role in governing the electrical and magnetic properties of the perovskite-type oxides, it is important to have accurate methods for their determination. The absolute oxygen content, *i.e.* the degree of total oxidation, can most conveniently be analyzed by chemical methods, most of which are redox titrations carried out in a liquid phase.[33] Chemical methods give highly accurate results provided that impurity phases are not present in the samples. In addition to wet-chemical methods, thermogravimetric reduction has been widely used for the oxygen content analysis of transition metal oxides.[34]

In oxide structures where the same element is located in different atomic positions, oxidation state and coordination at a distinct position may be an important factor. This is particularly essential with cuprate superconductors where the distribution of positive holes among the different copper-oxide layers is likely to affect the superconductivity properties.[6] Since chemical methods only give the average oxidation state of the metals, other methods are needed to obtain information on the oxidation states of distinct metal atoms in the structure. Element-specific methods such as XANES[35-43] and Mössbauer spectroscopies[44-49] are of great advantage owing to the possibility to selectively examine the chemical environment of a distinct element. Furthermore, oxygen positions and their occupancies in the crystal structure can be directly determined by structure refinement using neutron diffraction data (see *e.g.* Refs. 3 and 50). X-ray photoelectron spectroscopy, which is known to be a convenient technique for analyzing different oxidation states of metals, has only been of limited use in studying mixed oxidation states of copper due to the close $2p_{3/2}$ binding energies of Cu(II) and Cu(III).[51,52]

2.1 Chemical methods for the oxygen content analysis

In wet-chemical methods, the redox chemistry characteristic of transition metals is utilized. As a general procedure, the high-valent transition metal ions in the sample are reduced by a suitable reductant present in excess in the solution. The amount of unreacted reductant or the amount of a product formed in the reduction reaction is a measure of the "total average oxidation state" of the metals in the sample and is determined by titration. The most commonly used wet-chemical methods for the analysis of transition metal oxidation states are iodometric, cerimetric and coulometric titrations whose applicabilities depend on the sample studied.

Iodometric titration is probably the most widely used chemical method for the oxygen content analysis of transition metal oxides.[33] It is based on the reduction of high-valent ions in an acidic solution by KI, which reduces transition metal ions to their low-valent iodides. Iodine formed in the reactions is titrated by a thiosulphate solution using starch as an indicator. Iodometric titration is suitable for oxides of cobalt, copper and/or manganese but is not suitable for iron containing oxides.[15,16,18,19,53,54] In the cerimetric titration the high-valent ions of iron or cobalt are reduced by a known excess of Fe^{2+} ions and the unreacted Fe^{2+} ions are titrated by a cerium sulphate solution using ferroin as an indicator.[13,29,54] On the other hand, the reduction of high-valent copper by water rather than by Fe^{2+} disturbs the cerimetric analysis of copper oxides.[54]

Coulometric titration is the most versatile wet-chemical method for the analysis of the higher oxidation states of transition metals in their oxides.[33,54] It is based on the reduction of high-valent cations or peroxide-type oxygen with a known excess of monovalent copper (Cu(I)/(II) titration) or divalent iron (Fe(II)/(III) titration) in an acidic solution.[33] The unreacted part of Cu(I) or Fe(II) is oxidized by constant current and the amount of the species titrated is calculated from the time required for the oxidation according to Faraday's law. The coulometric titration system is presented in Figure 2. Coulometric titration method has also been successfully applied for the determination of the oxidation state of a metal in a structure with two different mixed-oxidation-state metals, *e.g.* for the determination of the oxidation state of lead in the presence of mixed-valent copper.[55] Due to its accuracy and versatility coulometric Cu(I)/(II) titration was used in the present study for the determination of the oxygen contents in the $Cu(Ba_{0.8}Sr_{0.2})_2(Yb_{1-x}Ca_x)Cu_2O_{6+z}$ ($0 \leq x \leq 0.35$, $0 < z < 1$) triple perovskites[I,II] and the Ba*RE*$(Fe_{0.5}Cu_{0.5})_2O_{5+\delta}$ double perovskites.[IV,V]

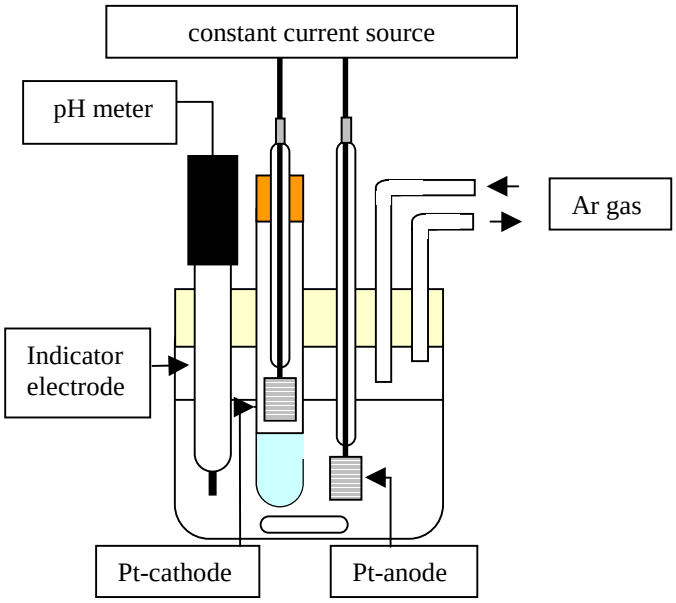

Figure 2. Coulometric titration cell.[33]

Thermogravimetry is a technique often used in studying oxygen non-stoichiometry and absolute oxygen contents in perovskite-type transition metal oxides. For the absolute oxygen content the sample is reduced in a thermobalance by a 5 % H_2/Ar gas mixture at a temperature of ~ 950 °C.[34] In a step-wise reduction process, transition metal is reduced to metallic, *e.g.* Cu, or to a low-valent oxide, *e.g.* FeO, whereas alkaline earth and rare earth elements stay as binary oxides.[IV,V,54] If the reduction products are known, the oxygen content can be calculated from the total weight loss. Furthermore, thermogravimetric heat treatments under argon or oxygen atmosphere can be used to study reversible changes in the oxygen content as also shown in the present work.[IV-VI]

2.2 Site-specific methods

2.2.1 Neutron diffraction

As the X-ray diffraction process depends on the number of electrons contributing to a (Bragg) reflection and varies with the angle of diffraction, light elements are difficult to detect in the presence of heavy elements. Therefore, X-ray diffraction is of limited use in studying the fine structure of perovskite oxides with small variations in oxygen stoichiometry. While X-rays are scattered by electrons, neutrons are scattered by the atomic nuclei. The scattering power of a nucleus for neutrons varies erratically in the periodic table and is independent of the angle. Neutron diffraction is a valuable method for examining a structure for the location and occupancy of oxygen atoms since the neutron scattering power of oxygen is relatively strong.[56] Structure refinement of neutron diffraction data gives phase-specific information about the location and the amount of the excess oxygen. Precise structural data obtained from the structure refinement can further be used for the estimation of the oxidation state of each ion with the bond-valence-sum (BVS) method.[57,58]

The present neutron powder diffraction (NPD) measurements of the $Cu(Ba_{0.8}Sr_{0.2})_2(Yb_{1-x}Ca_x)Cu_2O_{6+z}$ samples were carried out at the R2 reactor in Studsvik, Sweden.[I] The neutron powder diffractometer consisting of a double Cu (220) monochromator system (λ = 1.470 Å) and 35 ^{3}He detectors spaced 4.00° apart from each other, was used for the precise structure determination by scanning in steps of 0.08° over the 2θ range of 4.00-139.92°. The neutron scattering lengths for the elements in the $Cu(Ba_{0.8}Sr_{0.2})_2(Yb_{1-x}Ca_x)Cu_2O_{6+z}$ system are collected in Table 1.[56]

Table 1. Neutron scattering lengths used in the refinements of the $Cu(Ba_{0.8}Sr_{0.2})_2(Yb_{1-x}Ca_x)Cu_2O_{6+z}$ samples.[56]

Element	Cu	Ba	Sr	Yb	Ca	O
Neutron scattering length [fm]	7.718	5.07	7.02	12.430	4.70	5.803

2.2.1.1 *Rietveld method for structure refinement*

In the Rietveld method the entire diffraction profile, *i.e.* intensities of both diffraction peaks and the background, are utilized for the structure refinement of powder diffraction data.[59,60] The calculated powder diffraction pattern is compared point by point to the experimental diffraction pattern and selected parameters defining the structural model and describing the profile are adjusted by a least-squares method to give the best fit.[59] The quantity minimized in refinement is the residual sum

$$S_y = \sum_i w_i (y_i - y_{ci})^2 \qquad (1)$$

where w_i is the corresponding weight, y_i is the observed intensity at step i and y_{ci} is the calculated intensity at step i.[59] Each intensity value in a measurement can be calculated by summing contributions of all Bragg reflections and background at step i as

$$y_{ci} = S\sum_{hkl} (L_{hkl} \left|F_{hkl}\right|^2 \Phi(2\theta_i - 2\theta_{hkl}) P_{hkl} A) + I_{cb} \qquad (2)$$

where S is the scale factor,

L_{hkl} contains the Lorenz correction and multiplicity factors,

F_{hkl} is the structure factor,

$\Phi(2\theta_i - 2\theta_{hkl})$ is the reflection profile function,

P_{hkl} is the preferred orientation function,

A is an absorption factor and

I_{cb} is the background intensity.

In the structure refinement, the powder diffraction pattern is calculated taking into account instrument-related factors, *i.e.* the instrumental profile function, zero position, background, wave length and sample holder, and the sample-related factors, which include atomic coordinates, occupancies, temperature factors, lattice parameters, absorption and crystallite size. The peak shape is usually fitted with a simple Gaussian function or with a pseudo-Voigt function, which allows flexible variation of the Gaussian and Lorenzian character of the peak shape.[60] Several criteria can be used to describe the agreement between the measured and the calculated powder diffraction patterns. The definitions of the commonly used agreement

factors are shown in Table 2. R_{wp} is the most meaningful parameter because the numerator is the residual which is minimized in the refinement while χ^2 is considered a measure of the fit and convergence.[61]

The present structure refinements were carried out using either the tetragonal *P*4/*mmm* or the orthorhombic *Pmmm* space group for the triple perovskites of the $Cu(Ba_{0.8}Sr_{0.2})_2(Yb_{1-x}Ca_x)Cu_2O_{6+z}$ system.[I] The Rietveld program FullProf[62] was used for the refinements. Starting values for the cell parameters were taken from the X-ray refinement, and were refined together with the total scaling factor, the zero position and the background as first parameters. Atomic coordinates were first refined for the metal and then for the oxygen atoms. The same starting values for the coordinates of all atoms were used throughout both sample series. The shape of the peaks was refined using a Pseudo-Voigt function. Isotropic thermal displacement parameters, initially set at 1.5 $Å^2$, were refined for the metal atoms and for the oxygen atoms with full occupancy. For the partially occupied O(1) site the temperature factor was fixed at 0.3 in order to obtain a reliable estimation of the amount of excess oxygen. Refinement of the partial occupancies of the *Q* and *A* sites was found not to improve the fit and therefore the occupancies were fixed to their nominal values. Scale factor and cell parameters were in some cases refined for the impurity phase Yb_2BaCuO_5 but the contribution was less than 1 % and was thus not taken into account in the final refinements.[I]

Table 2. Definitions of the most commonly used agreement factors (%) in the Rietveld refinement.[61] *N* is the number of data points in the experimental powder diffraction profile and *P* is the number of parameters in the refinement.

R_p	R_{wp}	R_{exp}	χ^2
$= 100 \times \frac{\sum_i \lvert y_i - y_{ci} \rvert}{\sum_i \lvert y_i \rvert}$	$= 100 \times \left(\frac{\sum_i w_i (y_i - y_{ci}))^2}{\sum_i w_i y_i{}^2} \right)^{1/2}$	$= 100 \times \left(\frac{N - P}{\sum_i w_i y_i{}^2} \right)^{1/2}$	$= \left(\frac{R_{wp}}{R_{exp}} \right)^2$

2.2.1.2 *Bond-valence-sum method*

The bond-valence-sum rule developed by Brown and Altermatt[57,58] describes the correlation between the bond length and the bond valence. The bond valence s_{ij} of an *i-j* bond is calculated from an empirically determined parameter R_{ij}^0, specific for each *i-j* pair, and from the experimental bond length R_{ij} (in Å) as

$$s_{ij} = exp[(R_{ij}^{0} - R_{ij})/0.37] \quad . \tag{3}$$

Summing over the bond valences from all the nearest-neighbouring counter ions *j* gives the bond-valence sum of an ion *i* as

$$V_i = \pm\sum_j s_{ij} \quad . \tag{4}$$

The calculated bond-valence sum V_i reflects the oxidation state of ion *i* and is usually given as a positive value for the metal atoms and as a negative value for the oxygen atoms. The R_{ij}^0 value depends on the oxidation states of the *i* and *j* ions and is best obtained for an ion with an intermediate oxidation state by iterating[63] between the limit values tabulated by Brown and Altermatt.[57]

The BVS method allows for an estimation of the oxidation state of an ion based on the structural environment, *i.e.* the coordination sphere and the nearest-neighbouring atoms. BVS calculations can also be used for indicating tensile or compressive strain directed to an atom in a structure and further, for estimating compatibility of structural layers, *e.g.* in layered perovskite-type structures. Structural strains are indicative of the tendency of a structure to bind more oxygen or to release an oxygen atom since the strain can be discharged by changes in bond lengths.[58]

In the study of cuprate superconductors the BVS method has been of valuable use since it provides a tool to estimate the oxidation state of copper in different crystallographical positions based on the bond lengths calculated from the results of neutron diffraction refinement.[58,63,64] The appearance of superconductivity is often related to high-valent copper in the superconductive CuO_2 planes but the positive holes may also reside on oxygen or be

smoothly distributed in the metal-oxygen bond. Thus, to estimate the concentration of positive holes in the CuO_2 planes it is preferable to consider the bond-valence sums of both copper and oxygen atoms of the plane and sum them as[6,63]

$$p(CuO_2) = V_{Cu(2)} + V_{O(2)} + V_{O(3)} + 2 \quad . \tag{5}$$

2.2.2 O *K*-edge and Cu $L_{2,3}$-edge XANES spectroscopy

The energy region just below an absorption edge in the X-ray absorption spectrum contains information about the excitations of the inner-core electrons to the empty states in outer orbitals. In the XANES technique this pre-edge absorption region is used to extract information on the local electronic structure of individual atoms in the structure. XANES has shown to be a valuable method for the investigation of the concentration of unoccupied states at the copper and oxygen sites in superconductive copper-oxide structures.[35,36] This was successfully demonstrated by Nücker *et al.*[35] who showed that the multiple pre-edge peaks in the O *K*-edge spectrum of the $CuBa_2YCu_2O_{6+z}$ structure originate from the different binding energies of O 1*s* levels of the unequivalent oxygen sites. In the XANES studies of mixed copper oxides, the absorption spectra on Cu $L_{2,3}$- and O *K*-edges are most commonly analyzed but some Cu *K*-edge XANES studies have also been reported.[42,43] Quantitative information about the distribution of positive holes in the $CuA_2QCu_2O_{6+z}$ triple perovskite can be obtained by O *K*-edge XANES.[II] In the present work, the Cu $L_{2,3}$-edge and O *K*-edge XANES results of the $Cu(Ba_{0.8}Sr_{0.2})_2(Yb_{1-x}Ca_x)Cu_2O_{6+z}$ system are compared to the results obtained by the bond-valence sum calculations based on neutron diffraction data.[I,II] The analysis of the XANES spectra was performed in a way parallel to that reported in Refs. 35-41.

The O *K*-edge and Cu $L_{2,3}$-edge XANES measurements were carried out on the 6-m High-Energy Spherical Grating Monochromator beam-line at Synchrotron Radiation Research Center in Hsinchu, Taiwan. Details of the experiments are given in Publication II.

Interpretation of the O K-edge and Cu $L_{2,3}$-edge spectra

The O *K*-edge spectrum is obtained in the energy range of about 525-555 eV where the transition of the O 1*s* core electrons to holes with 2*p* character occurs below about 532 eV.[39] When the crystal structure of the studied material is known, the differences in the binding energies of electrons can be estimated using local-density-approximation (LDA) band-structure calculations.[35,65] In the $CuA_2QCu_2O_{6+z}$ triple perovskite the relative O 1*s* binding energies are highest for O(2) and decrease relative to O(2) by 0.1 – 0.7 eV in the order O(3), O(1) and O(4) (see Figure 1a for the notation of atomic sites).[35] In practice, the contributions of the in-plane oxygen atoms O(2) and O(3) are superimposed as well as the contributions of O(1) and O(4). Intensities of these two peaks, obtained by fitting Gaussian functions to each spectrum, are supposed to reflect the hole concentrations in the CuO_z chain and the two CuO_2 planes.

The Cu $L_{2,3}$-edge spectrum is obtained in the energy range of about 925-960 eV. The L_3 peaks have higher intensities than the L_2 peaks and consequently the L_3 peaks were used in the analysis. The contribution from divalent copper is seen at 931 eV whereas the absorption peak at 934 eV results from monovalent copper. Trivalent copper is seen as a shoulder on the high-energy side of the peak at 931 eV. In the present analyses, Cu $L_{2,3}$-edge XANES was mainly used for qualitative examination of the changes in the copper oxidation state in the Ca-substitution and O-doping sample series of the $Cu(Ba_{0.8}Sr_{0.2})_2(Yb_{1-x}Ca_x)Cu_2O_{6+z}$ system.[II]

2.2.3 ^{57}Fe Mössbauer spectroscopy

Mössbauer spectroscopy is based on emission and absorption of recoilless γ radiation by a Mössbauer active nucleus, *e.g.* ^{57}Fe.[44] It provides information on the local environment of the Mössbauer active nucleus in the structure since the energy levels of a nucleus depend on the surrounding lattice. The changes in the interaction between the nucleus and its environment are seen as small changes in the energies absorbed by the nucleus. The types of interaction are *i*) chemical interaction, *ii*) electric quadrupole interaction and *iii*) magnetic hyperfine interaction. As a consequence of a change in the binding or oxidation state of the nucleus, the chemical interaction is changed and the peak positions are shifted in the spectrum. Quadrupole interaction is related to the symmetry of the nucleus and therefore is indicative of the coordination of the nucleus. Interaction between the magnetic moment of the nucleus and

the external magnetic field effective at the nucleus is seen as splitting of the energy states which thus provides information on magnetic ordering of the material.[44]

Among the elements having a Mössbauer active nucleus, ^{57}Fe and ^{151}Eu are the most widely utilized in studying superconductive and related perovskite oxides.[44-49] The usefulness of Mössbauer spectroscopy is due to the possibility of substituting a cation in a superconductive structure by a Mössbauer active nucleus, *e.g.* ^{57}Fe-for-Cu substitution, which thereby allows the analysis of the environment of the cation position. If iron is present in different crystallographical positions, the proportion of each can be determined by analyzing the intensity of each spectral component. In the present work, ^{57}Fe Mössbauer spectroscopy was utilized in studying the oxidation states of Fe and Cu in the normal- and high-pressure heat-treated Ba*RE*$(Fe_{0.5}Cu_{0.5})_2O_{5+\delta}$ double perovskite with varying *RE* and δ.[VII]

3. MULTIVARIATE DATA ANALYSIS

The crystallographic fine structure of superconductive copper oxides determines the amount of positive holes in the CuO_2 planes and the charge distribution over the unit cell which are factors strongly believed to define the superconductivity properties. The fine structure can be described by several structural variables, such as metal-oxygen bond lengths, cation-cation distances and bond angles, all of which are strongly correlated to each other. Consequently, the appearance of superconductivity can be considered a multivariate problem.

Multivariate problems can be approached by so-called projection methods which allow both qualitative and quantitative examination of correlations between variables. The "principal component analysis" (PCA) method provides us with a qualitative means of examining correlations in a multivariate data set containing *N* observations and *K* variables.[66] "Principal components" (PC) are linear combinations of the initial variables and the first PC is the line which best approximates the group of data points. The second PC is orthogonal to the first PC and is determined to improve the approximation of the data variation as much as possible. Two PCs define a plane which can be considered a window into the *K*-dimensional space and, by projecting all the points onto the plane, the structure of the original data set is visualized in two dimensions. PC analysis can be used for searching trends, outliers, dominating variables, groups and clusters among the data. The "Projections to Latent Structures by means of partial least squares" (PLS) method is an extension of the PC analysis and is used when information on the dependence between *x* and *y* variables is desired. The relative importance of each variable on a selected *y* can be evaluated and furthermore, quantitative prediction of *y* is possible for a new observation. A detailed description of PCA and PLS is found in Ref. 66.

In the present work, PCA was used for the qualitative evaluation of relations between structural variables (such as the metal-oxygen bond lengths, bond angles and oxygen content *z*) and the T_c, of $MA_2QCu_2O_{6+z}$ phases with various compositions.[III] The data were adopted from a number of neutron diffraction studies published for these phases. The results are discussed together with the neutron diffraction refinement results of the $Cu(Ba_{0.8}Sr_{0.2})_2(Yb_{1-x}Ca_x)Cu_2O_{6+z}$ system in Chapter 4.2. Quantitative modeling of the value of T_c in the $CuA_2QCu_2O_{6+z}$ system was performed by PLS.[III]

4. CONTROL OF CHARGE DISTRIBUTION IN $CuA_2QCu_2O_{6+z}$ TRIPLE PEROVSKITES

4.1 Principles of hole-doping routes

In layered structures, the concentration of positive or negative carriers within each layer can be estimated by summing the bond-valence sums of cations and anions of the layer as in Equation (5). When considering the ways of controlling the carrier concentration within one layer, the in-plane bonds are found to counteract as an anion and a cation bonded to each other get the same bond-valence values with opposite signs.[67] Based on this fact, the carrier concentration of each layer can only be affected by changing the off-plane bonds with stoichiometry modifications. In superconductive copper oxides with a two-CuO_2-plane unit cell, the positive holes can be produced by three different mechanisms, *i.e.* by shortening the Cu(2)-O(4) bond or by lengthening the effective *A*-O(2,3) or *Q*-O(2,3) distance (Figure 3).[67,68] In the effective *A*/*Q*-O distance not only the bond length but also the corresponding R^0 value is taken into account, which means that both the oxidation state and the size of the *A*/*Q* substitute are considered. These three different ways, which were defined as hole-doping routes Π(1), Π(2) and Π(3), respectively, may work either individually or simultaneously in a structure.[67,68] Thus, the hole concentration of a CuO_2 plane, defined in Equation (5), can be expressed by individual bond valences as[67]

$$\begin{aligned} p(CuO_2) &= s_{Cu(2)\text{-}O(4)} + 4s_{Cu(2)\text{-}O(2,3)} - 2(2s_{Cu(2)\text{-}O(2,3)} + 2s_{A\text{-}O(2,3)} + 2s_{Q\text{-}O(2,3)}) + 2 \\ &= s_{Cu(2)\text{-}O(4)} - 4s_{A\text{-}O(2,3)} - 4s_{Q\text{-}O(2,3)} + 2 \end{aligned} \quad (6)$$

Note that, for an orthorhombic unit cell O(2) and O(3) are different. The net hole concentration value $p(CuO_2)$ can be divided to partial hole concentrations Π(1), Π(2) and Π(3) as[67]

$$p(CuO_2) = \Pi(1) + \Pi(2) + \Pi(3) \quad (7)$$

$$\Pi(1) = s_{Cu(2)\text{-}O(4)} \quad (8)$$

$$\Pi(2) = -4s_{A\text{-}O(2,3)} + 1 \quad (9)$$

$$\Pi(3) = -4s_{Q\text{-}O(2,3)} + 1. \quad (10)$$

The Π values have no meaning as absolute values but they provide us with a means of examining quantitatively the contribution of each hole-doping route on the total hole doping. For studying the functioning of hole-doping routes, the $Cu(Ba_{0.8}Sr_{0.2})_2(Yb_{1-x}Ca_x)Cu_2O_{6+z}$ triple-perovskite system was found advantageous since hole doping by different routes is achieved in the same structure by modifying either the oxygen or cation stoichiometry.[69] Without calcium substitution (*i.e.* $x = 0$), the $Cu(Ba_{0.8}Sr_{0.2})_2(Yb_{1-x}Ca_x)Cu_2O_{6+z}$ structure becomes superconductive when z exceeds 0.45 and the T_c reaches the maximum value of 82 K near $z \approx 1$. In the structure with no excess oxygen (*i.e.* $z = 0$) substitution of Yb by Ca leads to superconductivity when x exceeds 0.2, thus leaving a wide superconductive region $0.2 \leq x \leq 0.35$ for investigation.[69] In this substitution range, the T_c value increases to 43 K when x reaches 0.35. In the $CuBa_2(Y_{1-x}Ca_x)Cu_2O_{6+z}$ system, examination of the hole-doping routes is more limited due to the narrow solid-solubility range of Ca for Y ($0 \leq x \leq 0.2$).[70-72] It should be noted that, for the superconductive copper-oxide structures with more than two CuO_2 planes the hole doping routes for the outer and inner planes are different as described in Ref 6.

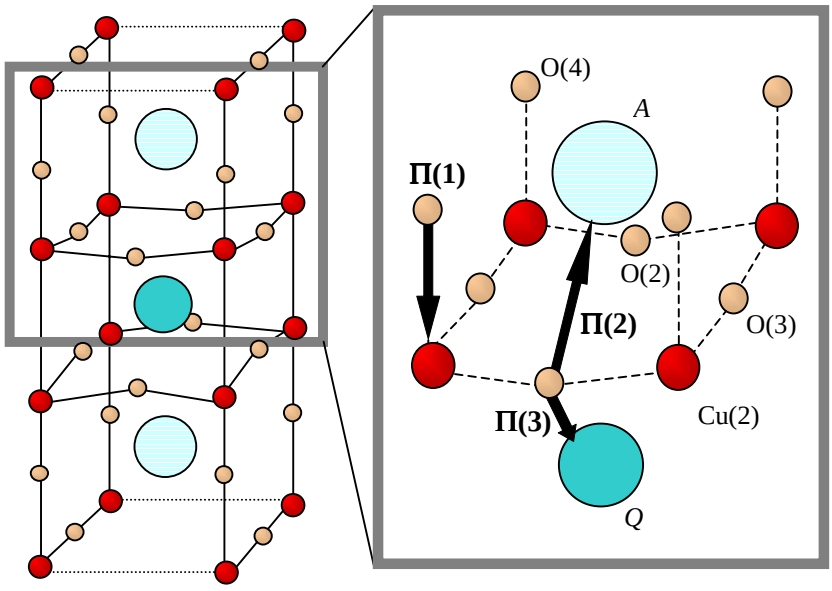

Figure 3. Hole-doping routes Π(1), Π(2) and Π(3) into a CuO_2 plane of $CuA_2QCu_2O_{6+z}$.[69]

4.2 Structural changes in $CuA_2QCu_2O_{6+z}$ *via* oxygen doping and Ca substitution

According to the neutron diffraction refinements of the $Cu(Ba_{0.8}Sr_{0.2})_2YbCu_2O_{6+z}$ samples with oxygen contents $0< z < 1$, incorporation of oxygen into the CuO_z chain results in a shift of apical oxygen O(4) towards the CuO_2 plane (route Π(1)) and Ba/Sr away from the in-plane oxygen atoms O(2) and O(3) (route Π(2)) as the oxidation proceeds.[I] As expected, the mechanism is similar to that found in the early studies of the $CuBa_2YCu_2O_{6+z}$ system.[3,48] The finding is further in accordance with the result of the present principal component analysis of the $CuA_2QCu_2O_{6+z}$ structure with various compositions which showed strong correlation among the oxygen content z, the T_c and the distances A-O(2), A-O(3) and Cu(2)-O(4).[III]

Substitution of trivalent Yb by divalent Ca in the $Cu(Ba_{0.8}Sr_{0.2})_2(Yb_{1-x}Ca_x)Cu_2O_{6+z}$ series ($z \approx 0$) increases the hole concentration in the CuO_2 plane by lengthening the effective (Yb,Ca)-O(2,3) bond according to route Π(3).[I] In the principal component analysis, the effects of Ca(II)-for-*RE*(III) substitution at the Q site are explained mainly by the parameter V_Q (V(Q) in Publication III) which is the average valence of the Q cation. V_Q has a negative correlation with the T_c, while the Q-O(2,3) bond length, which increases not only with Ca substitution but also with the size of the trivalent Q cation, does not directly correlate with the T_c.[III]

4.3 Distribution of holes in the $Cu(Ba_{0.8}Sr_{0.2})_2(Yb,Ca)Cu_2O_{6+z}$ lattice

Based on the bond-valence-sum calculations and XANES measurements, the holes created by oxygen doping and calcium substitution are distributed in a different way between the CuO_2 plane in the CuO_2-Yb/Ca-CuO_2 block and the CuO_z chain.[I,II] Hole doping by oxygen oxidizes mostly the CuO_z chain and directs only a part of the holes to the CuO_2 plane as judged from the Cu $L_{2,3}$-edge XANES spectrum (Figure 2 in Publication II). Calcium substitution increases the amount of holes in the CuO_2 plane with an efficiency higher than that of oxygen doping which is explained by the location of calcium between the two CuO_2 planes apart from the CuO_z chain. However, the CuO_z chain is also to some extent oxidized by Ca substitution as judged from the changes in the $p(CuO_2)$ values ($\Delta p(CuO_2)$ values obtained from neutron diffraction refinements and O K-edge XANES measurements in Publications I and II) which are smaller than the values calculated from the chemically analyzed oxygen content.[I,II]

The T_c is more efficiently increased as a function of $\Delta p(CuO_2)$ when the holes are doped by Ca substitution than by O doping. Furthermore, the two different hole-doping routes result in different relations between $\Delta p(CuO_2)$ or T_c and the in-plane Cu-O bond. This is an indication of other important factors in determining the T_c besides the hole concentration of the CuO_2 plane. One possible factor could be the distribution of holes in the Cu-O bond.[73] From the R^0 values of Cu(+III)-O(-II) (R^0 = 1.73 Å) and Cu(+II)-O(-I) (R^0 = 1.59 Å) bonds[57] it is concluded that the shorter the Cu-O bond is the smaller the R^0 value should be and the more the bond would have Cu(+II)-O(-I) character.[67,68] At a certain $\Delta p(CuO_2)$ value the in-plane Cu-O bond was found to be shorter in the Ca-substituted samples than in the O-doped samples.[I] Another possible meaningful parameter for the superconductivity properties may be buckling of the CuO_2 plane which was found to diminish by Ca substitution and to increase by O doping. The principal component analysis of the literature data on the $CuA_2QCu_2O_{6+z}$ phases showed negative correlation between the T_c and the flatness of the CuO_2 plane.[III]

4.4 Quantitative modeling of T_c and the fine structure of $CuA_2QCu_2O_{6+z}$

Structure-property relations modeling by PLS has so far been applied mainly to organic compounds, see *e.g.* Refs 74-77, but the method was found to be feasible for modeling structure-property relations of inorganic oxide structures as well.[III] Extending the multivariate data set to cover structural data and the values of different superconductivity properties of a variety of superconductive copper-oxide structures could allow evaluation of the structural parameters of the overall optimum superconductive compound. As the present study demonstrates, the data collected with different neutron diffraction instruments and analyzed by different research groups can be treated as a single data set. The possibility of using all available structural data in multivariate modeling is a prerequisite to creating a structure-property model for a large group of compounds.[III]

In general, the predictive power of a PLS model is determined by three factors, *i.e.* by the choice of the variables and the training set, and by the accuracy of the data used for training the model. In the present study, the T_c values for the under-doped $CuA_2QCu_2O_{6+z}$ samples are well predicted by the PLS model obtained but the values predicted for the over-doped samples are not reliable (Figure 4). This is quite understandable, since the T_c cannot be explained just by the crystallographical variables used in the present analysis. Consequently, the fully-

oxygenated Ca(II)-for-*Q*(III) substituted samples were clearly recognized over-doped with the predicted T_c values higher than the observed ones. Some inaccuracy in the modeling may be due to inexactness in the oxygen content values reported in different studies since the amount of excess oxygen in the structure is the most crucial variable affecting the value of T_c. The T_c values reported may also contain some variation depending on the measurement technique used. Furthermore, an important factor to be considered in the future studies is how to treat the data of compositionally different non-superconductive samples for which the T_c value was set at 0 K in the present analysis.[III]

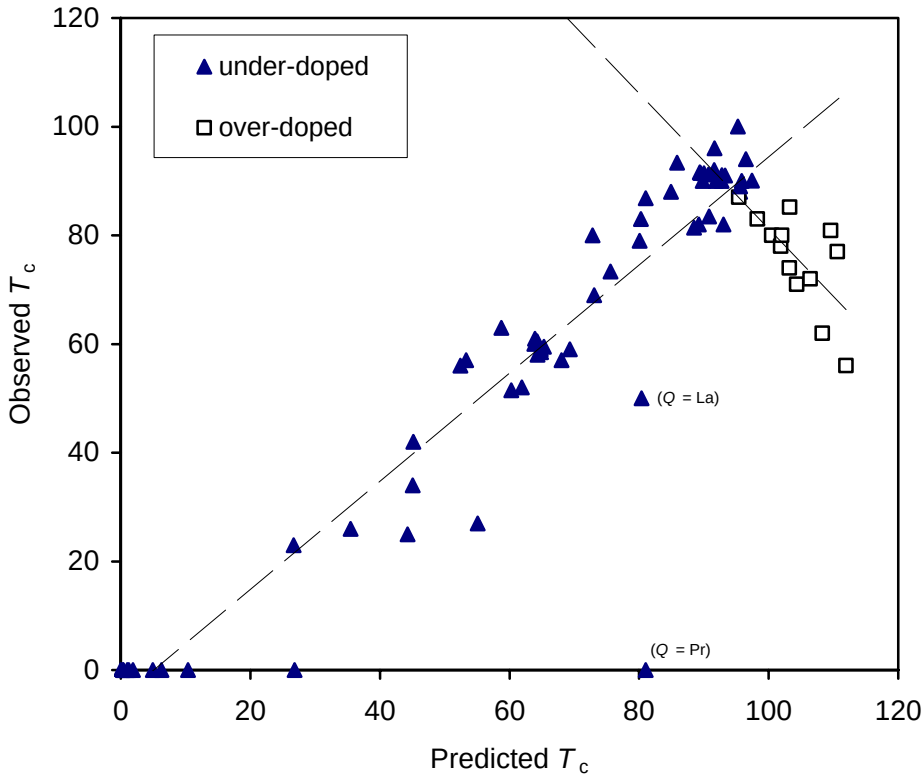

Figure 4. Predicting T_c of $CuA_2QCu_2O_{6+z}$ superconductors with a PLS model.[III]

5. CONTROL OF CHARGE DISTRIBUTION IN Ba*RE*$(Fe,Cu)_2O_{5+\delta}$ DOUBLE PEROVSKITES

The double perovskites in the Ba*RE*$(Fe_{1-x}Cu_x)_2O_{5+\delta}$ system have been a subject of research due to their electrical and magnetic properties which can be controlled by changing the Fe-to-Cu ratio and the oxygen stoichiometry. The iron-free phase would resemble closely the superconductive copper oxide structures and has been predicted to be superconductive with suitable tailoring.[7] The double-perovskite structure is more isotropic than the complicated layer structures of copper oxide superconductors which would be beneficial from the point of view of practical applications of high-T_c superconductivity. However, the oxygen excess in the *RE* layer in between the basal planes of the $(Fe,Cu)O_5$ pyramids would most probably destroy the superconductive properties and it has also been shown to weaken the magnetoresistive effect observed in the Cu-free phase.[7]

5.1 Formation of Ba*RE*$(Fe,Cu)_2O_{5+\delta}$ double perovskites

In the Ba*RE*$(Fe,Cu)_2O_{5+\delta}$ system, only the Ba*RE*$(Fe_{0.5}Cu_{0.5})_2O_{5+\delta}$ stoichiometry leads to the formation of a double-perovskite structure under ambient conditions. According to the latest neutron and electron diffraction studies of Ba*RE*$(Fe_{0.5}Cu_{0.5})_2O_{5+\delta}$, iron and copper are disordered within the $(Fe,Cu)O_2$ planes and the tetragonal structure possesses the space group *P*4/*mmm*.[78-81] However, the atomic positions of Fe and Cu are slightly different since the position of Fe is shifted towards the apical oxygen while Cu is located on the basal plane of the $(Fe,Cu)O_5$ pyramid.[78] Consequently, a CuO_5 pyramid is connected to a FeO_5 pyramid *via* the apical oxygen over the BaO layer. On the other hand, the two pyramids facing each other over the *RE* layer may contain any combination of Fe and Cu (Fe-Fe, Fe-Cu or Cu-Cu). From the rare earths, only scandium, lanthanum and cerium were found not to form the double-perovskite structure with the Ba*RE*$(Fe_{0.5}Cu_{0.5})_2O_{5+\delta}$ stoichiometry.[IV-VI]

Difficulties in synthesising Ba*RE*$(Fe_{1-x}Cu_x)_2O_{5+\delta}$ double perovskites with $x \neq 0.5$ are due to the redox and coordination characteristics of iron and copper.[7,13] Divalent iron in square pyramidal coordination is stabilized under reducing conditions only, while formation of trivalent copper requires high external pressure. The iron-rich BaSm$(Fe_{1-x}Cu_x)_2O_{5+\delta}$ double perovskites with x = 0, 0.05, 0.1 and 0.4 have been synthesized with the so-called

encapsulation technique in which the oxygen partial pressure is controlled with a metal getter.[14] Recently, the totally Cu-free double perovskite has been synthesized in reducing conditions also with other rare earths.[13,82] The Ba*RE*$Fe_2O_{5+\delta}$ samples with $\delta \approx 0$ accommodate oxygen when kept in air since divalent iron tends to be oxidized. Furthermore, the range of oxygen content variation is wide due to the possibility of iron to get oxidized to oxidation states higher than +III in the structure. The structure is either tetragonal *P*4/*mmm* or distorted to orthorhombic *Pmmm* except with the $\delta = 0.5$ stoichiometry which leads to ordering of oxygen and the space group *Pmna*.[13]

The formation of copper-rich double perovskites is limited by the strong preference of copper to occur as divalent rather than trivalent in the square pyramidal coordination. In the hypothetic iron-free "Ba*RE*$Cu_2O_{5.0}$" double perovskite, copper would have an average oxidation number of +2.5 which is higher than usually observed for copper in the square pyramidal coordination.[6] Thus, a charge-compensating substitution of divalent Ba by trivalent La is necessary to increase the relative amount of Cu from 50 %, and to tune the copper oxidation state in the square pyramids of the structure.[23] However, attempts to substitute La(III)-for-Ba(II) or Ca(II)-for-*RE*(III) in the Ba*RE*$(Fe,Cu)_2O_{5+\delta}$ double perovskite have so far been of limited success due to the formation of impurity phases in the synthesis.[83]

Since the square pyramidal coordination is favorable for Cu(II), Fe(III), Co(II) and Co(III), the Ba*REB*$_2O_5$ double perovskite is readily formed with combinations of these cations as long as the average oxidation state of the *B* site is at least +2.5. The range of oxygen content variation depends on the type of the *B*-site metal and the size of *RE*. Like high-valent iron in Ba*RE*$(Fe_{0.5}Cu_{0.5})_2O_{5+\delta}$, high-valent cobalt in Ba*RE*$Co_2O_{5+\delta}$ double perovskites has proven to be formed only in the structures with a large-sized *RE*, *i.e.* Nd an Pr[15], whereas manganese may exist as Mn(II), Mn(III) and Mn(IV) even in $BaYMn_2O_{5+\delta}$.[19] The formation of a simple perovskite structure is favoured with stoichiometries of $Ba_{0.5}La_{0.5}Fe_{0.5}Co_{0.5}O_{3-w}$ and $Ba_{0.5}La_{0.5}MnO_{3-w}$ but annealing these perovskites under reducing conditions has been found to lead to the ordering of La and Ba and to the formation of a double-perovskite structure.[12,18]

5.2 Normal- and high-pressure treatment of Ba*RE*$(Fe_{0.5}Cu_{0.5})_2O_{5+\delta}$ double perovskites

Under normal pressure, the stabilization of an excess oxygen atom in the *RE* layer of Ba*RE*$(Fe_{0.5}Cu_{0.5})_2O_{5+\delta}$ double perovskites is possible in the structures with *RE* = Nd or Pr only.[IV,V] Heat treatment under an ultra-high pressure of 5 GPa stabilizes the excess oxygen (δ = 0.05 ~ 0.20) also in the structures with smaller-sized *RE*s (Figure 5). The excess oxygen content can be tuned continuously by heat treatments under a deoxidative atmosphere. The oxygen evolution characteristics are similar to those observed for the $CuBa_2RECu_2O_{6+z}$ triple perovskite, even though the chemical environment of the excess oxygen atom in the two structures is different. The distribution of the "total oxidation" between copper and iron in Ba*RE*$(Fe_{0.5}Cu_{0.5})_2O_{5+\delta}$ was determined by comparing the changes in the ^{57}Fe Mössbauer spectra to those observed in the chemically analyzed oxygen content values. In the normal-pressure oxygenation of Ba*RE*$(Fe_{0.5}Cu_{0.5})_2O_{5+\delta}$ (*RE* = Nd, Pr), the excess oxygen atom enters the position between two FeO_5 pyramids (Fe-Fe) or a FeO_5 and a CuO_5 pyramid (Fe-Cu) whereas high-pressure heat treatment directs the excess oxygen atom with equal probability to the positions between Fe-Fe, Fe-Cu and Cu-Cu. Consequently, in the normal-pressure oxygenation iron is oxidized to higher oxidation states while under high pressure part of copper is oxidized to the trivalent state as well.[VII]

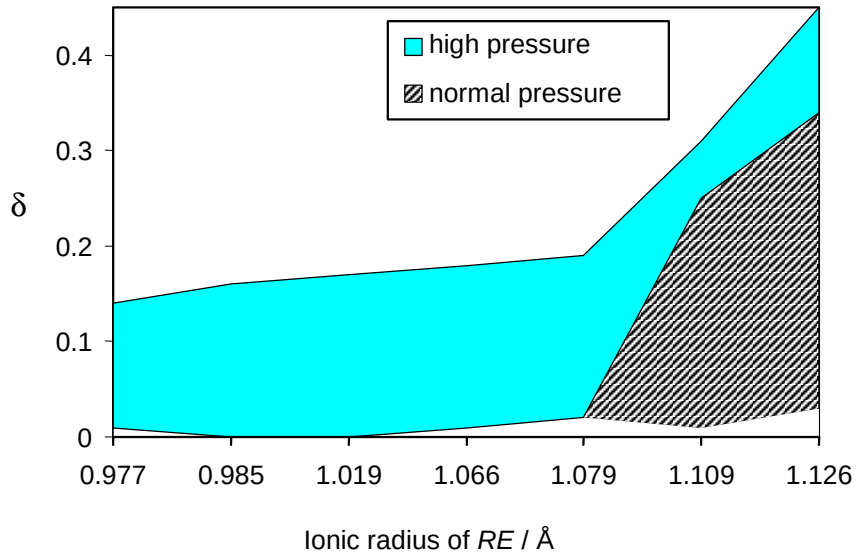

Figure 5. Oxygen stoichiometry variations in the Ba*RE*$(Fe_{0.5}Cu_{0.5})_2O_{5+\delta}$ series upon normal-pressure and high-pressure heat treatments.[V]

Magnetic properties of Ba*RE*$(Fe_{0.5}Cu_{0.5})_2O_{5+\delta}$ double perovskites are greatly affected by the oxidation states of iron and copper. The stoichiometric Ba*RE*$(Fe_{0.5}Cu_{0.5})_2O_5$ is antiferromagnetic, independent of the *RE* constituent, while the normal-pressure oxygenated structures (*RE* = Nd or Pr) are paramagnetic at room temperature.[VIII] In the samples synthesized under normal pressure, the Néel temperature decreases with increasing amount of excess oxygen in the lattice. Besides the antiferromagnetic-to-paramagnetic transition, a weak spontaneous magnetization at T_2 was observed, which is probably due to reordering of iron magnetic moments in the direction of the *c* axis.[VIII,24] The complex ordering results from slightly different positions of copper and iron within the $(Fe,Cu)O_2$ plane which prevents ordering of the magnetic moments parallel to the *c* axis. Similar ordering has also been found in the Ba*RE*$(Co_{1-x}Cu_x)_2O_5$ double perovskites ($0.38 < x < 0.5$).[84] The high-pressure heat-treated Ba*RE*$(Fe_{0.5}Cu_{0.5})_2O_{5+\delta}$ double perovskites are antiferromagnetic at room temperature although the oxygen content is higher than in the samples oxygenated under normal pressure.[VIII] This supports the finding that under high pressure, copper accepts part of the oxidation and the antiferromagnetic coupling of high-spin trivalent iron spins is less affected by the excess oxygen. Furthermore, no magnetic transition at T_2 was found to occur in the high-pressure heat treated BaY$(Fe_{0.5}Cu_{0.5})_2O_{5+\delta}$. This was proposed to be due to iron and copper positions becoming identical as the high-pressure treatment directs excess oxygen to the coordination sphere of copper as well.[VIII,24]

6. CONCLUSIONS

Understanding the relationship between the fine structure and charge distribution is required for controlling material properties and tailoring new materials with perovskite-type structures. In the present work, a systematic approach was taken to evaluate the different ways of tuning the oxidation states of iron and copper in distinct atomic sites in the CuA_2RECu$_2$O$_{6+z}$ triple-perovskite and the BaRE(Fe$_{0.5}$Cu$_{0.5}$)$_2$O$_{5+\delta}$ double-perovskite structures. In conclusion, control of the transition metal oxidation states is achieved *i*) by tuning the oxygen stoichiometry, *ii*) by making cation substitutions and/or *iii*) by applying external pressure in the synthesis.

The present work demonstrates how the information obtained by different methods of analysis can be combined to determine the charge distribution over the unit cell of layered multi-metal oxides. Coulometric titration was applied for the analysis of the "total average oxidation" of iron and/or copper in the structures while the distribution of charge between unequivalent transition metal sites was determined by site-specific methods such as neutron diffraction, Cu $L_{2,3}$- and O K-edge XANES and ^{57}Fe Mössbauer spectroscopy. The different methods used in the present work are summarized in Figure 6.

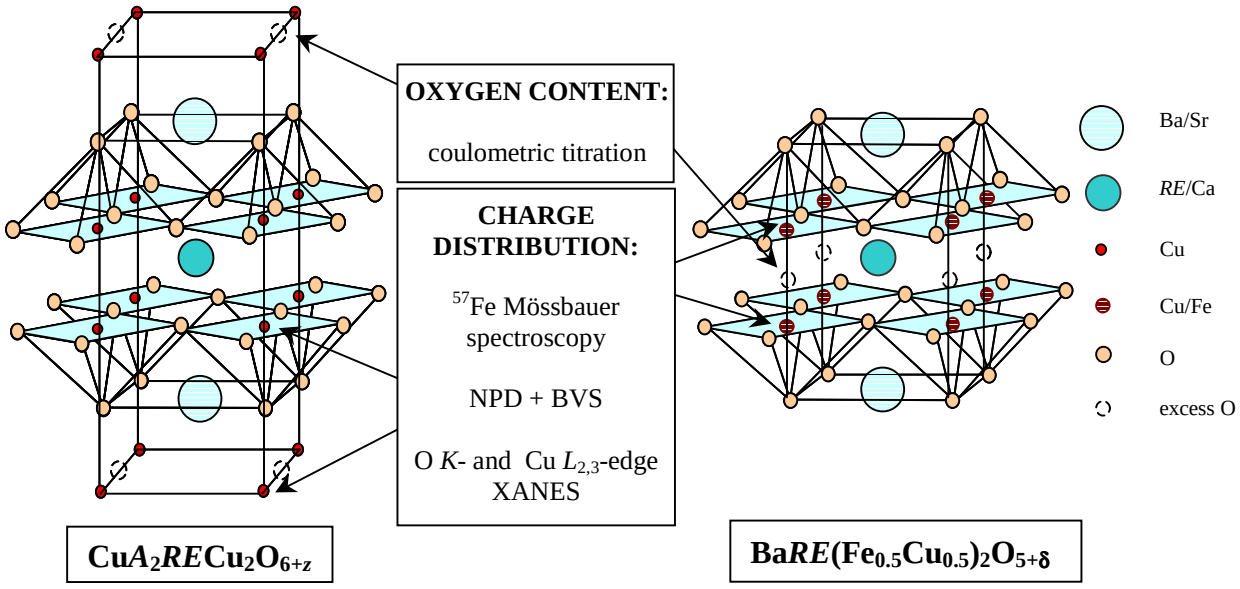

Figure 6. Methods used for the determination of iron and copper oxidation states in the CuA_2RECu$_2$O$_{6+z}$ triple perovskite and the BaRE(Fe$_{0.5}$Cu$_{0.5}$)$_2$O$_{5+\delta}$ double perovskite. The arrows point to the location of the excess oxygen atom and the transition metal atoms sharing the positive holes in the structures.

XANES results of the charge distribution in the CuO_2 plane and in the CuO_z chain of the Ca(II)-for-Yb(III) substituted and O-doped $Cu(Ba_{0.8}Sr_{0.2})_2(Yb_{1-x}Ca_x)Cu_2O_{6+z}$ triple perovskites were in good agreement with the bond-valence-sum calculations based on neutron diffraction refinement. In the $CuA_2RECu_2O_{6+z}$ triple perovskite, the two ways of doping have a different effect on the fine structure, and consequently the distribution of positive holes between the two copper positions of the unit cell becomes different. In the $BaRE(Fe_{0.5}Cu_{0.5})_2O_{5+\delta}$ double perovskite, oxygen doping by normal-pressure oxygenation oxidizes iron only, while after high-pressure heat treatment both iron and copper are oxidized, as judged from the results of ^{57}Fe Mössbauer spectroscopy. Multivariate data analysis was applied for the first time to illustrate correlations between fine structure and properties of oxide materials.

REFERENCES

1. Raveau, B., Michel C., Hervieu, M., and Groult D., *Crystal Chemistry of High-T_c Superconducting Copper Oxides*, Springer-Verlag, Berlin 1991, 331 p.

2. Wu, M.K., Ashburn, J.R., Torng, C.J., Hor, P.H., Meng, R.L., Gao, L., Huang, Z.J., Wang, Y.Q., and Chu, C.W., *Phys. Rev. Lett.* **58** (1987) 908.

3. Cava, R. J., Hewat, A. W., Hewat, E. A., Batlogg, B., Marezio, M., Rabe, K. M., Krajewski, J. J., Peck Jr., W. F., and Rupp Jr., L. W., *Physica C* **165** (1990) 419.

4. Huang, Q., Karen, P., Karen, V.L., Kjekshus, A., Lynn, J.W., Mighell, A.D., Rosov, N., and Santoro, A., *Phys. Rev. B* **45** (1992) 9611.

5. Geremia, S., Nardin, G., Mosca, R., Randaccio, L., and Zangrando, E., *Solid State Commun.* **72** (1989) 333.

6. Karppinen, M. and Yamauchi, H., *Mater. Sci. Eng. R* **26** (2000) 51.

7. Yamauchi, H. and Karppinen M., *Physica C* **335** (2000) 273.

8. Er-Rakho, L., Michel, C., Lacorre, Ph., and Raveau, B., *J. Solid State Chem.* **73** (1988) 531.

9. Pissas, M., Mitros, C., Kallias, G., Psycharis, V., Simopoulos, A., Kostikas, A., and Niarchos, D., Synthesis, *Physica C* **192** (1992) 35.

10. Barbey, L., Nguyen, N., Caignaert, V., Hervieu, M., and Raveau, B., *Mater. Res. Bull.* **27** (1992) 295.

11. Rentschler, T., *J. Alloys Comp.* **232** (1996) 43.

12. Minet, Y., Lefranc, V., Nguyen, N., Domengés, B., Maignan, A., and Raveau, B., *J. Solid State Chem.* **121** (1996) 158.

13. Karen, P. and Woodward, P.M., *J. Mater. Chem.* **9** (1999) 789.

14. Nakamura, J., Lindén, J., Karppinen, M., and Yamauchi, H., *Appl. Phys. Lett.* **77** (2000) 1683.

15. Maignan, A., Martin, C., Pelloquin, D., Nguyen, N., and Raveau, B., *J. Solid State Chem.* **142** (1999) 247.

16. Martin, C., Maignan, A., Pelloquin, D., Nguyen, N., and Raveau, B., *Appl. Phys. Lett.* **71** (1997) 1421.

17. Zhou, W., Lin, C.T., and Liang, W.Y., *Adv. Mater.* **5** (1993) 735.

18. Millange, F., Caignaert, V., Domenges, B., Raveau, B., and Suard, E., *Chem. Mater.* **10** (1998) 974.

19. Millange, F., Suard, E., Caignaert, V., and Raveau, B., *Mater. Res. Bull.* **34** (1999) 1.

20. Chapman, J.P., Attfield, J.P., Mölgg, M., Friend, C.M., and Beales, T.B., *Angew. Chem. Int. Ed. Engl.* **35** (1996) 2482.

21. Beales, T.B., Mölgg, M., Jutson J., and Friend, C.M., *Phys. Stat. Sol. A* **161** (1997) 271.

22. Lehmus, K., *Licentiate (Tech) Thesis*, Helsinki University of Technology, Espoo 2000, 64 p.

23. Nagase, M., Lindén, J., Suematsu, H., Karppinen, M., and Yamauchi, H., *Phys. Rev. B* **59** (1999) 1377.

24. Nagase, M., Lindén, J., Miettinen, J., Karppinen, M., and Yamauchi, H., *Phys. Rev. B* **58** (1998) 3371.

25. Libby, W.F., *Science* **171** (1971) 499.

26. Pena, M.A. and Fierro, J.L.G, *Chem. Rev.* **101** (2001) 1981-2017.

27. Tokura, Y. and Tomioka, Y., *J. Magn. Magn. Mater.* **200** (1999) 1.

28. Maignan, A., Martin, C., and Raveau, B., *J. Supercond*. **13** (2000) 313.

29. Lindén, J., Karen, P., Kjekshus, A., Miettinen, J., Pietari, T., and Karppinen, M., *Phys. Rev. B* **60** (1999) 15251.

30. Awana, V.P.S., Nakamura, J., Lindén, J., Karppinen, M., and Yamauchi, H., *Solid State Commun.* **119** (2001) 159.

31. Suard, E., Fauth, F., Caignaert, V., Mirebeau, I., and Baldinozzi, G., *Phys. Rev. B* **61** (2000) 11871.

32. Vogt, T., Woodward, P.M., Karen, P., Hunter, B.A., Henning, P., and Moodenbaugh, A.R., *Phys. Rev. Lett.* **84** (2000) 2969.

33. Karppinen, M., Fukuoka, A., Niinistö, L., and Yamauchi H., *Supercond. Sci. Technol.* **9** (1996) 121.

34. Karppinen, M., Niinistö, L., and Yamauchi, H., *J. Therm. Anal.* **48** (1997) 1123.

35. Nücker, N., Pellegrin, E., Schweiss, P., Fink, J., Molodtsov, S. L., Simmons, C. T., Kaindl, G., Frentrup, W., Erb, A., and Müller-Vogt, G., *Phys. Rev. B* **51** (1995) 8529.

36. Chen, J.M., Liu, R.G., Chung, S.C., Liu, R.S., Kramer, M.J., Dennis, K.W., and McCallum, R.W., *Phys. Rev. B* **55** (1997) 3186.

37. Merz, M., Nücker, N., Pellegrin, E., Schweiss, P., Schuppler, S., Kielwein, M., Knupfer, M., Golden, M.S., Fink, J., Chen, C.T., Chakarian, V., Idzerda, Y.U., and Erb, A., *Phys. Rev. B* **55** (1997) 9160.

38. Chen, J.M., Liu, R.S., Lin, J.G., Huang, C.Y., and Ho, J.C., *Phys. Rev. B* **55** (1997) 14586.

39. Liu, R.S., Chang, C.Y., and Chen, J.M., *Inorg. Chem.* **37** (1998) 5527.

40. Liu, R.S., Chang, C.Y., Chen, J.M., and Liu, R.G., *J. Supercond.* **11** (1998) 563.

41. Chen, J.M., Liu, R.S., Nachimuthu, P., Kramer, M.J., Dennis, K.W., and McCallum, R.W., *Phys. Rev. B* **59** (1999) 3855.

42. Bianconi, A., DeSantis, M., Di Ciccio, A., Flank, A.M., Fronk, A., Fontaine, A., Legarde, P., Yoshida, H.K., Kotani, A., and Marcelli, A., *Phys. Rev. B* **38** (1988) 7196.

43. Choy, J.-H., Kim, D.-K., Hwang, S.-H. and Demazeau, G., *Phys. Rev. B* **50** (1994) 16631.

44. Lindén, J., *Doctoral Thesis*, Helsinki University of Technology, Espoo 1994, 41 p.

45. Lindén, J., Hietaniemi, J., Ikonen, E., Lippmaa, M., Tittonen, I., Karlemo, T., Karppinen, M., Niinistö, L., and Ullakko, K., *Phys. Rev. B* **46** (1992) 8534.

46. Lindén, J., Lippmaa, M., Miettinen, J., Tittonen, I., Katila, T., Kareiva, A., Karppinen, M., Niinistö, L., Valo, J., and Leskelä, M., *Phys. Rev. B.* **50** (1994) 4154.

47. Lindén, J., Lippmaa, M., Miettinen, J., Tittonen, I., Katila, T., Karppinen, M., and Niinistö, L., *Phys. Rev. B.* **50** (1994) 16040.

48. Lindén, J., Lippmaa, M., Karen, P., Kjekshus, A., and Karppinen, M., *J. Solid State Chem.* **138** (1998) 87.

49. Lindén, J., Kjekshus, A., Karen, P., Miettinen, J., and Karppinen, M., *J. Solid State Chem.* **139** (1998) 168.

50. Jorgenssen, J.D., Veal, B.W., Paulikas, A.P., Nowicki, L.J., Crabtree, G.W., Claus, H., and Kwok, W.K., *Phys. Rev. B* **41** (1990) 1863.

51. Ihara, H., Hirabayashi, M., Terada, N., Kimura, Y., Senzaki, K., Akimoto, M., Bushida, K., Kawashima, F., and Uzuka, R., *Jpn. J. Appl. Phys.* **26** (1987) L460.

52. Karppinen, M., Yamauchi, H., Suematsu, H., Isawa, K., Nagano, M., Itti, R., and Fukunaga, O., *J. Solid State Chem.* **130** (1997) 213.

53. Huang, Q., Karen, P., Karen, V.L., Kjekshus, A., Lynn, J.W., Mighell, A.D., Natali Sora, I., Rosov, N., and Santoro, A., *J. Solid State Chem.* **108** (1994) 80.

54. Salomäki, K., *M.Sc. Thesis*, Helsinki University of Technology, Espoo 2001, 72 p.

55. Karppinen, M., Yamauchi, H., and Tanaka, S., *J. Solid State Chem.* **104** (1993) 276.

56. Rodriguez-Carvajal, J., Computer program "Fullprof" for structure refinement, cf. Ref. 62.

57. Brown, I.D. and Altermatt, D., *Acta Crystallogr.* **B41** (1985) 244.

58. Brown, I.D., *J. Solid State Chem.* **82** (1989) 122.

59. Rietveld, H., *J. Appl. Cryst.* **2** (1969) 65.

60. McCusker, L.B., Von Dreele, R.B., Cox, D.E., Louër, D., and Scardi, P., *J. Appl. Cryst.* **32** (1999) 36.

61. Harris, K.D.M. and Tremayne, M., *Chem. Mater.* **8** (1996) 2554.

62. Rodriguez-Carvajal, J., *PSI-Proc.* 93-01 (1993) 73.

63. Tallon, J. L., *Physica C* **168** (1990) 85.

64. De Leeuw, D.M., Groen, W.A., Feiner L.F., and Havinga, E.E., *Physica C* **166** (1990) 133.

65. Temmerman, W.M., Szotec, Z., and Guo, G.Y., *J. Phys. C* **21** (1988) L867.

66. Eriksson, L., Johansson, E., Kettaneh-Wold, N., and Wold, S., *Introduction to Multi- and Megavariate Data Analysis using Projection Methods (PCA & PLS)*, Umetrics Ab, Umeå 1999, 490 p.

67. Karppinen, M. and Yamauchi, H., *Phil. Mag. B* **79** (1999) 343.

68. Karppinen, M. and Yamauchi, H., *Int. J. Inorg. Mater.* **2** (2000) 589.

69. Fujinami, K., Karppinen, M., and Yamauchi, H., *Physica C* **300** (1998) 17.

70. Berastegui, P., Eriksson, S.-G., Johansson, L.G., Kakihana, M., Osada, M., Mazaki, H., and Tochihara, S., *J. Solid State Chem.* **127** (1996) 56.

71. Böttger, G., Mangelschots, I., Kaldis, E., Fischer, P., Krüger, Ch., and Fauth, F., *J. Phys. Cond. Matter* **8** (1996) 8889.

72. Awana, V.P.S., Malik, S.K., and Yelon, W.B., *Physica C* **262** (1996) 272.

73. Zheng, G., Kitaoka, Y., Asayama, K., Hamada, K., Yamauchi, H., and Tanaka, S., *Physica C* **260** (1996) 197.

74. Verhaar, H.J.M., Ramos, E.U., and Hermens, J.L.M., *J. Chemom.* **10** (1996) 149.

75. Sandberg, M., Eriksson, L., Jonsson, J., Sjöström, M., and Wold, S., *J. Med. Chem.* **41** (1998) 2481.

76. McCloskey, J.T., Newman, M.C., and Clark, S.B., *Environ. Toxicol. Chem.* **15** (1996) 1730.

77. Fleischer, R., Wiese, M., Troschütz, R., and Zink, M., *J. Mol. Model.* **3** (1997) 338.

78. Caignaert, V., Mirebeau, I., Bourée, F., Nguyen, N., Ducouret, A., Grenéche, J.M., and Raveau, B., *J. Solid State Chem.* **114** (1995) 24.

79. Suematsu, H., Nagase, M., Tomokiyo, Y., Karppinen, M., and Yamauchi, H., in *Advances in Superconductivity XI*, Koshizuka, N. and Tajima, S., (Eds.) Springer, Tokyo 1998, 389.

80. Ruiz-Aragón, M.J., Morán, E., Amador, U., Martínez, J.L., Andersen, N.H., and Ehrenberg, H., *Phys. Rev. B* **58** (1998) 6291.

81. Ruiz-Aragón, M.J., Amador, U., Morán, E., and Andersen, N.H, *Physica C* **235-240** (1994) 1609.

82. Nakamura, J., Karppinen, M., and Yamauchi, H., unpublished results.

83. Nagase, M., *M.Sc. Thesis*, Tokyo Institute of Technology, Tokyo 1998, 92 p.

84. Barbey, L., Nguyen, N., Caignaert, V., Studer, F., and Raveau, B., *J. Solid State Chem.* **112** (1994) 148.

HELSINKI UNIVERSITY OF TECHNOLOGY

INORGANIC CHEMISTRY PUBLICATION SERIES

No. 1 Nieminen, M.,
Deposition of Binary and Ternary Oxide Thin Films of Trivalent Metals by Atomic Layer Epitaxy. 2001.

No. 2 Putkonen, M.,
Development of Low-Temperature Deposition Processes by Atomic Layer Epitaxy for Binary and Ternary Oxide Thin Films. 2002.

ISBN 951-22-5920-6

ISSN 1458-5154